

Simultaneous broadband radio and optical emission of meteor trains imaged by LOFAR / AARTFAAC and CAMS

Tammo Jan Dijkema¹ , Cees Bassa¹ , Mark Kuiack² , Peter Jenniskens³ ,
Carl Johannink³, Felix Bettonvil⁴, Ralph Wijers² , Richard Fallows¹ 

¹ASTRON, Netherlands Institute for Radio Astronomy

²Anton Pannekoek Institute, University of Amsterdam

³SETI Institute

⁴Leiden University / NOVA

November 18, 2021

Abstract

We report on simultaneous 30 - 60 MHz LOFAR / AARTFAAC12 radio observations and CAMS low-light video observations of +4 to -10 magnitude meteors at the peak of the Perseid meteor shower on August 12/13, 2020. 204 meteor trains were imaged in both the radio and optical domain. Aside from scattered artificial radio sources, we identify broadband radio emission from many persistent trains, one of which lingered for up to 6 minutes. Unexpectedly, fewer broadband radio meteor trains were recorded when the experiment was repeated during the 2020 Geminids and 2021 Quadrantids. Intrinsic broadband radio emission was reported earlier by the Long Wavelength Array, but for much brighter meteors and observed with lower spatial resolution. The new results offer insight into the unknown radio emission mechanism.

1 Introduction

Meteors are well-known to reflect artificial radio emission in forward and backward scattering. Combined optical and radio meteor scatter observation of meteors go back to (Prentice et al., 1947), showing that meteor trains are overdense for most visible meteors. Forward meteor scatter, where transmitter and receiver are not at the same lo-

cation, can be used to study meteors as is done in, e.g., the Belgian Radio Meteor Stations (BRAMS) network (Lamy et al., 2011).

Less well established is the detection of intrinsic natural radio emission from the meteor or meteor train itself. Early efforts to detect intrinsic emission relied on temporal coincidences (e.g., (Price & Blum, 2000)). The first more substantive reports based on radio imaging came from all-sky imaging at low radio frequencies (~40 MHz) with the Long Wavelength Array, detecting intrinsic non-thermal radio emission from fireballs (Obenberger et al., 2014, 2016a,b). The emission persisted well after the meteor itself had faded. The emission mechanism of these meteor radio afterglows is not fully understood, and so far has not been independently confirmed with other instruments. A survey with the Murchison Widefield Array (Zhang et al., 2018) did not show this intrinsic emission at higher 72–103 MHz frequencies.

Several mechanisms for broadband radio emission from meteors have been suggested in the literature, namely reflected broadband terrestrial radio emission, intrinsic emission from chemically produced suprathermal electrons (Obenberger et al., 2020), Langmuir waves (Obenberger et al., 2015), free-free emission (Filonenko, 2018) and transition radiation (Obenberger et al., 2020). Also, bright celestial radio emission shines on the meteor trains and that radiation may be scattered, as suggested in

Obenberger et al. (2015).

Here we report on low-frequency all-sky observations with the LOFAR (“Low Frequency Array”) radio telescope (van Haarlem et al., 2013) during the 2020 Perseid meteor shower (Jenniskens, 2006). The radio data are complemented with simultaneous, both temporally and spatially, optical video observations from the CAMS BeNeLux network (Jenniskens et al., 2011) in an effort to study the altitude dependence of the proposed intrinsic radio emission.

2 Observations

The LOFAR radio telescope consists of thousands of dipole antennas grouped into stations spread over Europe, with a dense core of stations located in the North of the Netherlands. Each LOFAR station has low-band antennas (LBAs) which can observe from 10 to 90 MHz and high-band antennas (HBAs) operating from 110 to 250 MHz. During regular LOFAR LBA observations radio signals are combined (beamformed) hierarchically, by first combining radio signals from dipole antennas in a station, and then combining or correlating the combined radio signals from stations to increase sensitivity at the expense of field-of-view.

The AARTFAAC piggyback instrument (Prasad et al., 2016; Kuiack et al., 2019, 2021) provides a special observing mode whereby LOFAR can create all-sky images of the radio sky. It does so by correlating the radio signals from all 576 LBA dipoles from the inner 12 LOFAR stations located in the dense core (with a 1.2 km diameter) surrounding the “super terp” in Drenthe, the Netherlands, see Fig. 1.

LOFAR/AARTFAAC observations were obtained during the Perseid meteor shower (2020 August 12-13) for 64 frequency channels of 48.8 kHz bandwidth (grouped into 16 subbands of 4 channels each), spread over radio frequencies between 30 to 60 MHz. These observations were used to create all-sky images with 3’ spatial resolution and 2 s time resolution.

All-sky radio images were created for each of the individual AARTFAAC subbands (a set of 4 channels). This analysis used a newer version of the pipeline described in Shulevski et al. (2021). As part of the pipeline, the brightest radio sources Cassiopeia A and Cygnus A were sub-

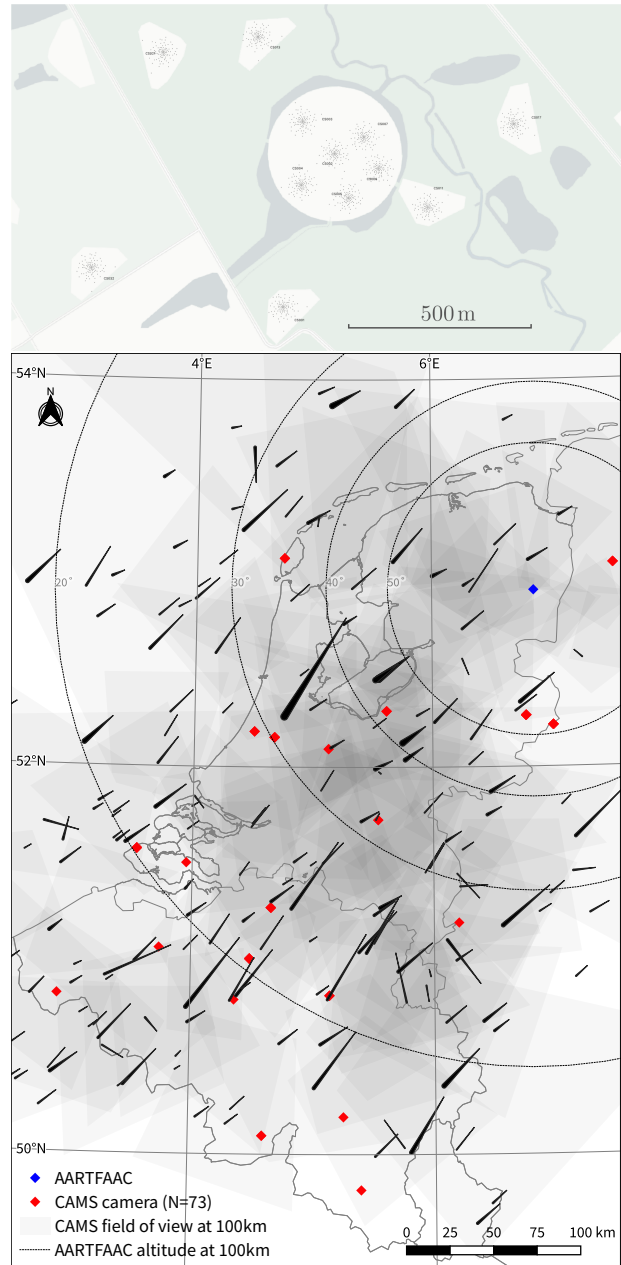


Figure 1: Top: map of the LOFAR core with the location of all 512 dipole antennas used for AARTFAAC. Bottom: map with CAMS camera locations (red), the location of the LOFAR core (blue) and co-observed meteors.

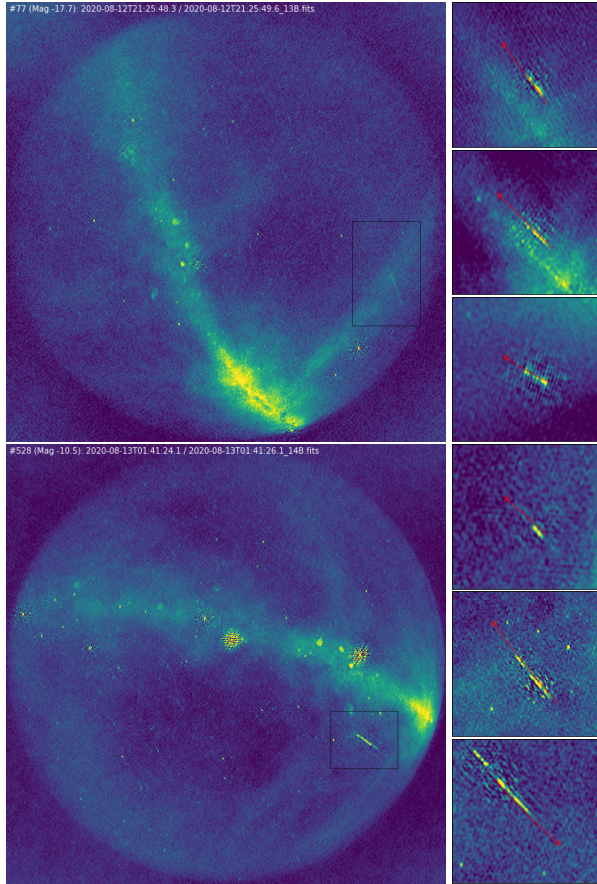


Figure 2: AARTFAAC image (integrated over all observing bands) of the meteors at 2020-08-12 21:25:48 UTC (top left) and 2020-08-13 01:41:24 UTC (bottom left). The large-scale diffuse emission is the Galactic plane, the bottom left image shows some residuals of the subtracted sources Cassiopeia A and Cygnus A. The right column shows zoomed in meteors, from top to bottom corresponding to numbers 144, 235, 249, 317, 333, and 704 in the CAMS data set. In red, the trajectory as computed from the CAMS optical observations is overlaid.

tracted, to minimize imaging artefacts across the all-sky images. Typically, in subbands containing strong narrow-band terrestrial radio emission reflected by meteor ionization trails, such as emission from the BRAMS meteor forward scatter network transmitter in Belgium near 50 MHz (Lamy et al., 2016), the imaging failed, and images from

these subbands were rejected. Images from the remaining subbands were averaged in radio frequency across subbands. This resulted in 10713 all-sky radio images at a 2 s cadence, corresponding to 5 h of data. Example all-sky images obtained with AARTFAAC are shown in Fig. 2. A full time-lapse of these images is available as Dijkema et al. (2021b).

The CAMS BeNeLux low-light video network is part of the global (“Cameras for Allsky Meteor Surveillance”) network and uses close to 100 low-light video cameras spread over the BeNeLux to triangulate optical meteors +4 and brighter using methods described in Jenniskens et al. (2011). Weather was clear during the night of 2020 August 12-13 and the trajectory and orbits of 720 meteors were measured (Roggemans, 2020).

Figure 2 shows a subset of these meteor trajectories overlaid on the all-sky radio images from the perspective of the “super terp”. All all-sky radio images within a few seconds of CAMS detections were inspected manually for radio emission coincident with the reconstructed meteor trajectory. This resulted in 204 meteors where radio emission was coincident with a CAMS detection. Of these meteors, 59 had a discernible trail in the radio images, the others showed up as point-like in the radio images. There were also dozens of radio meteors without a counterpart in the CAMS data, mostly due to missing sky coverage of CAMS in Germany at the time, see Fig. 1.

For each radio meteor coincident with a CAMS detection we have determined the begin and end point of the radio trail in the all-sky radio images and the duration for which the meteor was visible in the radio images.

3 Results

The coincidence of optical and radio trails demonstrates that meteors are a source of radio emission, be it scattering or intrinsic emission. That emission can last up to minutes; the longest radio train we have observed lasted 6.5 min, coincident with a CAMS meteor detection with optical magnitude of -9 . In general, we find that brighter optical meteors result in radio trains that remain visible for longer, as shown in Fig. 3a.

The detected radio emission is integrated over a 2-second time interval. Based on the decay of brightness in subsequent 2-s intervals, the short trails are mostly emis-

sion from the meteor’s persistent train, rather than from the meteor itself.

The optical trails of CAMS detected meteors start and end at higher altitudes for brighter meteors, and while the radio trains show a similar dependency (Fig. 3b and c), the radio emission is first detected at lower altitudes ($h = 101 \pm 4$ km) compared to optical emission ($h = 107 \pm 6$ km). The altitude at which the optical and radio emission ends is comparable for optical ($h = 94 \pm 6$ km) and radio ($h = 92 \pm 6$ km).

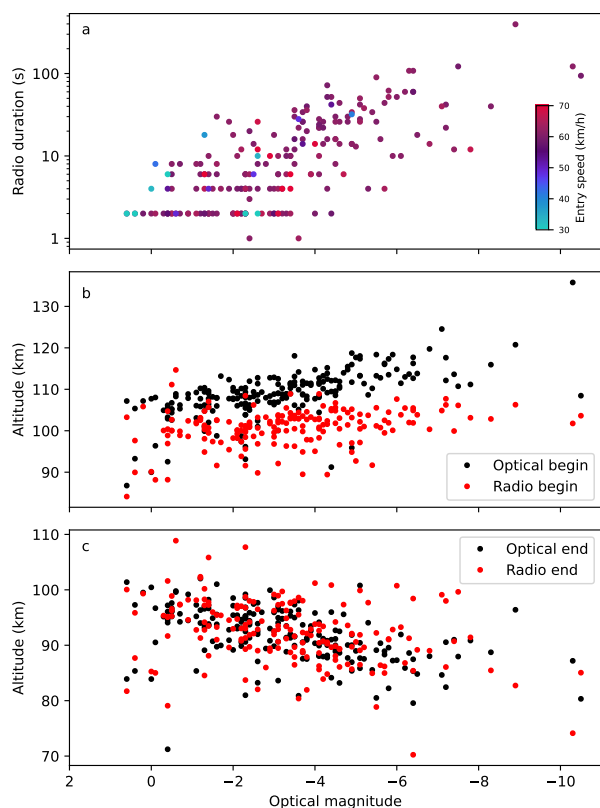


Figure 3: The dependency of the radio visibility and the altitude of the beginning and end of the meteor trail with optical brightness and entry speed. Note that the CAMS-derived peak optical brightness is less reliable below -5 magnitude due to video blooming.

Some of the radio trains that were persistent for several minutes were distorted by high altitude winds, much like

optical persistent trains. Figure 4 shows an example of the spatial evolution of the radio train with time. The peak intensity of the radio meteor train decreased over time.

Some frequency channels show reflected narrow-band artificial radio sources, but all channels contain a broadband radio component that is not likely from artificial radio sources. For bright radio meteors, the signal-to-noise ratio was sufficient to detect this broadband emission in almost all individual channels for frequencies below ~ 50 MHz. An example is shown in Fig. 4.

Further insight was obtained when repeating the AARTFAAC observations during the 2020 Geminid meteor and the 2021 Quadrantid meteor shower. Unfortunately, cloudy weather prevented simultaneous CAMS video observations. During that campaign, the all-sky radio images showed significantly fewer radio meteors compared to the observations of the Perseids.

4 Discussion

We can exclude an important contribution from forward scattered narrow band terrestrial radio emission, which is frequency resolved in our observations. Broadband emission would require a source of very broad band (30–50 MHz) terrestrial radio emission, which we consider unlikely.

Of the proposed intrinsic emission scenarios, chemically produced suprathermal electrons (Obenberger et al., 2020) could cause lingering radiation over minutes timescale if those electrons are captured by atoms and molecules that slowly diffuse into the train. Other proposed mechanisms such as Langmuir waves (Obenberger et al., 2015), free-free emission (Filonenko, 2018) and transition radiation (Obenberger et al., 2020), would be expected strong in the meteor itself, but we see the radiation increase in intensity following the meteor head before fading.

There are several possible reasons why fewer meteor trails were detected during the Geminids and Quadrantids. Geminids and Quadrantids are known to reach peak brightness at lower altitudes than the Perseids and show generally weaker optical persistent trains (Jenniskens, 2006). In our case, the lower entry velocities of the Geminids and Quadrantids in comparison to the Perseids is perhaps not to blame. We note that several slower sporadic

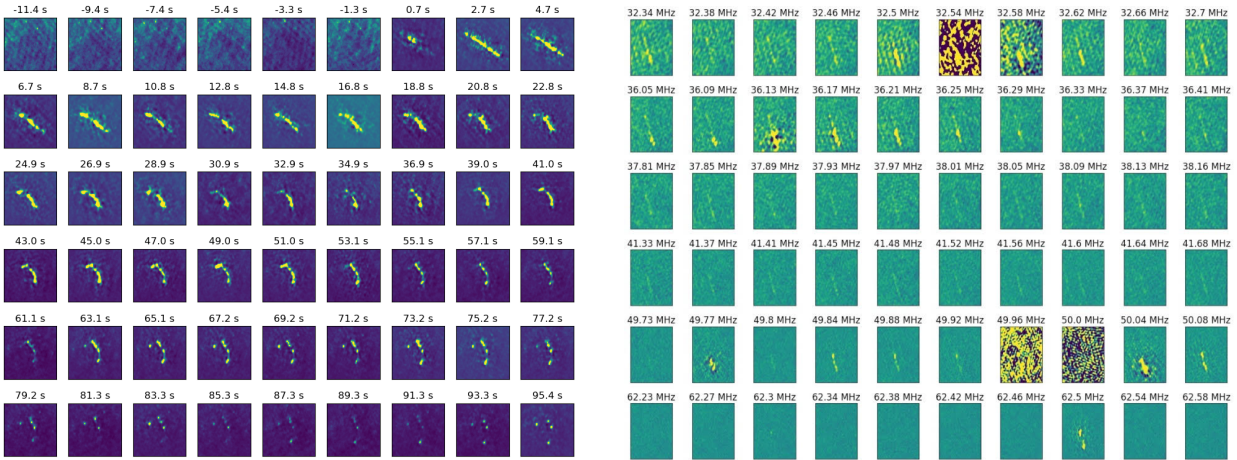


Figure 4: (Left:) The temporal and spatial evolution of a persistent radio meteor train, showing distortion by high altitude winds. The time is referenced to the beginning of the optical meteor trail. (Right:) Frequency evolution of a meteor train from a bright optical meteor. In channels where the emission from the meteor was very bright, the calibration has failed. That is the case in the bands where narrow-band terrestrial radio emission is reflected from the ionization train. Known transmitters operate at 32.54 MHz (TV transmitter), 49.97 and 49.99 MHz (reflection of the BRAMS meteor radars; [Lamy et al. 2016](#)) and 50.00 MHz (amateur radio transmissions).

meteors of similar brightness were observed in radio during the Perseids meteor shower, see Fig. 3a.

The atmospheric conditions may be important. During the Perseids, the summer weather provided hot and dry conditions, while the Geminids and Quadrantids were observed during the rainy winter season.

Finally, it is possible that the local sidereal time was important. The scattering of bright celestial radio sources, as suggested in [Obenberger et al. \(2015\)](#) was rejected in that paper with an argument involving the fact the earlier LWA detections are very bright. Since we have detected much weaker radio meteors, that argument does not hold here.

During the Perseids, the Galactic center and Galactic plane, which is the source of most low-frequency radio emission, was above the LOFAR horizon, while this was not the case during the Geminids and Quadrantids.

5 Conclusions

The AARTFAAC observations presented here show that persistent radio emission from meteors coincides with

their optical trajectories, and can be detected for meteors of magnitude ~ 0 and brighter. Aside from a narrow-band scattering of artificial radio sources, there is also a generally broadband emission detected for frequencies below 50 MHz. The continuum radio emission is first detected at lower altitudes compared to the optical emission, while both radio and optical emission end at similar altitudes. For the brightest optical meteors, we find that the radio emission can persist for several minutes. Persistent radio trains are affected by high altitude winds like the optical persistent trains.

Analysis of the AARTFAAC observations is ongoing, so it is currently not possible to distinguish between the suggested origins of the broadband radio emission.

Acknowledgements: We thank Albert van Duin and Edwin van Dijk for the use of facilities at the Edgar Gertruer Observatory in Burlage. We acknowledge interesting discussions with the researchers in the BRAMS project. We thank all camera operators and other contributors to CAMS-BeNeLux. PJ acknowledges support from NASA grant 80NSSC19K0563 (Solar System Workings).

Supplemental materials: Properties of the radio meteors observed simultaneously with CAMS are available as (Dijkema et al., 2021a).

References

- Dijkema, T. J., Bassa, C., Kuiack, M., et al. 2021a, Annotated data of simultaneous broadband radio and optical emission of meteor trains imaged by LOFAR / AARTFAAC and CAMS, Zenodo, doi: [10.5281/zenodo.5644202](https://doi.org/10.5281/zenodo.5644202)
- . 2021b, Time-lapse of AARTFAAC detections of radio meteors in Perseids 2020, 1.0, Zenodo, doi: [10.5281/zenodo.5595288](https://doi.org/10.5281/zenodo.5595288)
- Filonenko, A. D. 2018, *Geomagnetism and Aeronomy*, 58, 693, doi: [10.1134/S0016793218050055](https://doi.org/10.1134/S0016793218050055)
- Jenniskens, P. 2006, *Meteor Showers and their Parent Comets* (Cambridge University Press, Cambridge, UK), 790 pp
- Jenniskens, P., Gural, P. S., Dynneson, L., et al. 2011, *Icarus*, 216, 40, doi: [10.1016/j.icarus.2011.08.012](https://doi.org/10.1016/j.icarus.2011.08.012)
- Kuiack, M., Huizinga, F., Molenaar, G., et al. 2019, *MNRAS*, 482, 2502, doi: [10.1093/mnras/sty2810](https://doi.org/10.1093/mnras/sty2810)
- Kuiack, M., Wijers, R. A. M. J., Shulevski, A., et al. 2021, *MNRAS*, 505, 2966, doi: [10.1093/mnras/stab1504](https://doi.org/10.1093/mnras/stab1504)
- Lamy, H., Ranvier, S., Anciaux, M., et al. 2016, in *EGU General Assembly Conference Abstracts*, EGU General Assembly Conference Abstracts, EPSC2016–11624
- Lamy, H., Ranvier, S., de Keyser, J., et al. 2011, in *Meteoroids: The smallest solar system bodies. Proceedings of the Meteoroid Conference held in Breckenridge, Co, USA, May 24–28, 2010*, ed. W. J. Cooke, D. E. Moser, B. F. Hardin, & D. Janches, 551–356
- Obenberger, K., Taylor, G. B., & Holmes, J. M. 2016a, in *AGU Fall Meeting Abstracts*, P33E–06
- Obenberger, K. S., Dowell, J. D., Hancock, P. J., et al. 2016b, *Journal of Geophysical Research (Space Physics)*, 121, 6808, doi: [10.1002/2016JA022606](https://doi.org/10.1002/2016JA022606)
- Obenberger, K. S., Holmes, J. M., Ard, S. G., et al. 2020, *Journal of Geophysical Research (Space Physics)*, 125, e28053, doi: [10.1029/2020JA028053](https://doi.org/10.1029/2020JA028053)
- Obenberger, K. S., Taylor, G. B., Lin, C. S., et al. 2015, *Journal of Geophysical Research (Space Physics)*, 120, 9916, doi: [10.1002/2015JA021229](https://doi.org/10.1002/2015JA021229)
- Obenberger, K. S., Taylor, G. B., Hartman, J. M., et al. 2014, *ApJ*, 788, L26, doi: [10.1088/2041-8205/788/2/L26](https://doi.org/10.1088/2041-8205/788/2/L26)
- Prasad, P., Huizinga, F., Kooistra, E., et al. 2016, *Journal of Astronomical Instrumentation*, 5, 1641008, doi: [10.1142/S2251171716410087](https://doi.org/10.1142/S2251171716410087)
- Prentice, J. P. M., Lovell, A. C. B., & Banwell, C. J. 1947, *MNRAS*, 107, 155, doi: [10.1093/mnras/107.2.155](https://doi.org/10.1093/mnras/107.2.155)
- Price, C., & Blum, M. 2000, *Earth, Moon Planets*, 82–83, 545–554
- Roggemans, P. 2020, *eMeteorNews*, 5, 400
- Shulevski, A., Franzen, T. M. O., Williams, W. L., et al. 2021, arXiv e-prints, arXiv:2103.15160. <https://arxiv.org/abs/2103.15160>
- van Haarlem, M. P., Wise, M. W., Gunst, A. W., et al. 2013, *A&A*, 556, A2, doi: [10.1051/0004-6361/201220873](https://doi.org/10.1051/0004-6361/201220873)
- Zhang, X., Hancock, P., Devillepoix, H. A. R., et al. 2018, *Monthly Notices of the RAS*, 477, 5167, doi: [10.1093/mnras/sty930](https://doi.org/10.1093/mnras/sty930)